Organic Geochemistry 196 (2024) 104808

Contents lists available at ScienceDirect

Organic Geochemistry

journal homepage: www.elsevier.com/locate/orggeochem

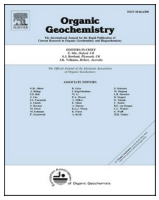

The stable sulfur isotope and abundance fluxes of reduced inorganic sulfur and organic sulfur phases recorded in the Permian-Triassic transition of the Meishan type section

Paul F. Greenwood [a,b,*], Hendrik Grotheer [a,1], Michael E. Böttcher [c,d], Kliti Grice [a]

[a] Western Australian Organic and Isotope Geochemistry Centre (WA-OIGC), School of Earth and Planetary Sciences, The Institute for Geoscience Research, Curtin University, GPO BOX U1987 Perth, WA 6845, Australia
[b] School of Earth and Environment, University of Western Australia, Crawley, WA 6009, Australia
[c] Geochemistry and Stable Isotope Biogeochemistry Group, Leibniz Institute for Baltic Sea Research (IOW), D-18119 Warnemünde, Germany
[d] Marine Geochemistry, University of Greifswald, D-17489, Greifswald, Germany Interdisciplinary Faculty, University of Rostock, D-18059, Rostock, Germany

ARTICLE INFO

Associate Editor — Lorenz Schwark

Keywords:
Sulfur
Cycle
Biochemistry
Compound specific
Organic sulfur compound
Kerogen
Mass extinction

ABSTRACT

Sulfur cycle fluxes implicated in the Permian-Triassic mass extinction have traditionally been studied by the sulfur phase abundances in sedimentary rocks and the stable sulfur isotopic value ($\delta^{34}S$) of seawater sulfate inferred from mineral sulfate analyses. This information might be complemented by studies of the reduced inorganic sulfur and organic sulfur produced following bacterial sulfate reduction. To explore this potential the $\delta^{34}S$ and concentration analyses of total reduced inorganic sulfur (TRIS) and organic sulfur – separately in the forms of kerogen (Ker) and individual organosulfur compounds, specifically dibenzothiophenes (DBTs) – has been conducted on sediments across the Late Permian to Early Triassic marine type section of Meishan-1 (South China). The relatively steady $\delta^{34}S$ profiles (e.g., < 5 ‰ variation) of all sulfur phases measured through much of the late Permian were indicative of a primary seawater sulfate control, but other biogeochemical modulators caused prominent $\delta^{34}S$ fluctuations of TRIS and DBT adjacent to the extinction event. The late Triassic $\delta^{34}S_{TRIS}$ profile of Meishan-1 displayed a notable ^{34}S enrichment (+15 ‰ increase) in bed 22–24 sediments concomitant with lower $\delta^{34}S_{DBT}$ values (−7 ‰ decrease), whereas co-eval $\delta^{34}S_{KerS}$ values remained relatively constant. The contrasting $\delta^{34}S_{DBT}$ and $\delta^{34}S_{KerS}$ data suggests the dynamic behavior of specific diagenetic sulfurisation processes may be resolved by the $\delta^{34}S$ of discrete organic sulfur compounds (i.e., dibenzothiophenes, DBTs), but dissipated by the sulfurisation collective represented by the bulk kerogen fraction. The inverse isotopic trend observed between DBT and TRIS resulted in negative $\Delta\delta^{34}S_{DBT\text{-}TRIS}$ values identifying an organic sulfurisation pathway(s) with an unusual preference over pyrite (FeS_2) for the lighter stable sulfur isotope. A redox control of the $\delta^{34}S_{DBTs}$ and $\delta^{34}S_{TRIS}$ deviations in the bed 22–24 extinction interval was confirmed by coincident variation in TRIS/(TRIS + KerS) and pyrite (Py) and highly reactive (HR) iron ratios (Fe_{Py}/Fe_{HR}). The iron (Fe) speciation data indicated a transition to ferruginous conditions, ruling out Fe^{2+} limitation as a factor in the bias against ^{34}S evident in DBT formation. The ^{34}S depletion of the DBTs promoted by the ferruginous setting may arise from the rapid and irreversible reaction of organic substrates with labile sulfur anions (e.g. HS^-) or be supported by an especially localised sediment–water depositional microenvironment. Our study highlights the potential of incorporating stable sulfur isotope analytics of reduced and organic sulfur phases, particularly of specific organic compounds, into a holistic assessment of the dynamic sulfur biochemical periods of Earth's past.

1. Introduction

The P-T extinction, when up to 95 % of all species on Earth vanished, marks a period of abrupt and profound environmental change on Earth and is popularly considered the most severe extinction during the Phanerozoic (Benton and Twitchett, 2003; Grice et al., 2005; Whiteside and Grice, 2016). Despite its prominent status there is still some conjecture about the actual cause of the P-T extinction. The two main

* Corresponding author.
E-mail address: p.greenwood@curtin.edu.au (P.F. Greenwood).
[1] Present address: Alfred Wegener Institute for Polar and Marine Research, Marine Geochemistry, 27568 Bremerhaven, Germany.

https://doi.org/10.1016/j.orggeochem.2024.104808
Received 30 January 2024; Received in revised form 22 April 2024; Accepted 24 May 2024
Available online 3 June 2024

explanations are changes in volcanic activity related to eruption of Siberian flood basalts (Bowring et al., 1998; Wignall, 2001) and global ocean occurrences of anoxic bottom waters and eutrophic surface water (Benton and Twitchett, 2003; Grice et al., 2005; Hallam and Wignall, 1997). These phenomena seriously impact the S-biogeochemical function of marine and terrestrial ecosystems and could account for the large S-cycle fluxes (e.g., S-isotopic composition of ocean sulfur reservoirs; Canfield and Teske, 1996) with the P-T extinction event as well as concurrent changes in global oxygen (O) and iron (Fe) cycles (Canfield and Teske, 1996; Newton et al., 2004).

Global sulfur (S) cycles during the P-T transition have been profiled by abundance and stable sulfur ($\delta^{34}S$) isotopic analyses of evaporites, carbonate associated sulfate (CAS) and pyrites recorded in sediments from a number of different geographical locations (Berner and Raiswell, 1983; Wilkin et al., 1996; Wignall and Newton, 1998; Newton et al., 2004; Kaiho et al., 2006a). It is widely accepted that the $\delta^{34}S$ value of seawater sulfate ($\delta^{34}S_{SO4}$) decreased through the Permian, recording a Phanerozoic minimum of near 10 ‰ close to the Permian Triassic Boundary (PTB), then inflects to a period of ^{34}S enrichment in the Early Triassic (Claypool et al., 1980; Chen and Chu, 1988; Newton et al., 2004; Bernasconi et al., 2017). Quite large fluctuations in $\delta^{34}S_{SO4}$ values very near to the PTB, or at the extinction horizon (Kaiho et al., 2006a), have been identified in several studies thus implicating a large S-flux event(s) in the actual mass extinction.

New insights into S-biochemical dynamics of paleo-environments may also be revealed from the isotopic and abundance characteristics of reduced S and organic S products that are primarily produced following microbial sulfate reduction, with the magnitude of S isotopic fractionation between these S-phases potentially indicative of variations in microbial metabolisms or disproportionation of S. The stable isotopic analysis of total reduced inorganic sulfur ($\delta^{34}S_{TRIS}$), often predominantly pyrite ($\delta^{34}S_{py}$) data has been included in several previous P-T studies and shown to fluctuate widely through the extinction event. To explore the complementary value the isotopic and content analyses of reduced inorganic S and organic S may bring to studies of the P-T extinction,and potentially other mass extinction events, here we have separately measured the abundance and $\delta^{34}S$ values of total reduced inorganic S (TRIS), kerogen S (KerS) and several different organic sulfur compounds (OSC; i.e., parent and methyl dibenzothiophenes) in the Late Permian to Early Triassic marine type section of the Meishan-1 (South China) drill core, encompassing the Global Stratotype Section and Point (GSSP). Sulfur isotope analyses of organic substrates has traditionally been limited to the analysis of kerogen (e.g., Passier et al., 1999; Werne et al., 2003), the non-solvent soluble fraction of organic sediments, which potentially contains a multitude of organic species produced from a variety of sulfurisation reactions. The emerging GC-ICPMS capability of continuous flow compound specific S isotope analysis (CSSIA; Amrani et al., 2009; Greenwood et al., 2014), however, presents a new opportunity to separately measure the $\delta^{34}S$ of different organic sulfur compounds which may relate to unique formation or transition processes. Here, the S isotope analytics were considered with established molecular biomarker and Fe speciation data which inform on water column redox conditions.

2. Meishan-1 marine type section

The GSSP has been thoroughly investigated in paleontological and geochemical studies of the P-T mass extinction at Meishan (Jin et al., 2000; Hongfu et al., 2001; Kaiho et al., 2001, 2006a; Cao et al., 2009, Cao and Zheng, 2009; Saito et al., 2023). The Meishan-1 core was drilled near the quarry Meishan Section D and comprised sediments containing the transition, the entire Changhsingian Stage and post-extinction Early Triassic Induan Stage (Cao et al., 2009). The Changhsingian Formation represents slope-to-basin facies comprised of graded beds of organic-rich calcarenite, marly micrite and radiolarian chert (Wignall and Hallam, 1993; Bowring et al., 1999; Jin et al., 2000; Cao and Zheng, 2009) – a detailed stratigraphic section with bed and drill core depth positions of presently studied Meishan-1 sediments can be found elsewhere (Cao et al., 2009).

The present study was conducted on a subset of 11 Meishan-1 drill core samples remaining from a previous study (Grice et al., 2005), including two samples each from beds 22, 24 and 26 (106.52–111.04 m) spanning the extinction transition. The End Permian Mass Extinction (EPME) is at the top of bed 24e and beginning of bed 25, identified from a disappearance of fossils and sharp decline in species richness (Jin et al., 2000) and spikes in Hg and terrestrial biomarkers (Grice et al., 2005; Kaiho et al., 2006a, 2020). Fluctuations in photosynthetic sulfur carotenoid biomarkers, attributed to periodic ocean euxina, have also been reported coincident with the EPME (Grice et al., 2005; Saito et al., 2023). The main extinction took place in as little as 100,000 years. The P-T boundary was marked at Bed 27c by the first occurrence of the conodont *Hindus Parvus* (Hongfu et al., 2001; Benton and Twitchett, 2003). The thermal maturity of organic matter in the Meishan-1 core has also been assessed – most reliably using the 22S/22S + 22R C_{31} homohopane ratio – as being uniformly in the earliest stages of the oil window (Cao et al., 2009), and thus unlikely to have significantly impacted the $\delta^{34}S$ values of inorganic or organic S species.

3. Analytical methods

3.1. Sample preparation

The bitumen fraction of the sediments (~5–25 g) was isolated by microwave extraction (x2) of the finely ground sediment sample in DCM:MeOH (9:1 v/v) at 80 °C. Activated copper was added to the bitumen extracts to remove elemental sulfur, which was found to be negligible. The bitumen were then separated by column chromatography over activated silica gel (120 °C) into aliphatic, aromatic and polar fractions using *n*-hexane, *n*-hexane:DCM (7:3; v/v) and DCM:MeOH (1:1; v/v) eluants, respectively. A S-rich aromatic sub-fraction was obtained by column chromatography over aluminum oxide (AlO^2; Type 507C neutral; Fluka) with three successive *n*-hexane:DCM eluants (99:1; 90:10; 0:100; the last of which gave the S-rich aromatic fraction; Grotheer et al., 2017).

3.2. GC–MS

The molecular composition of the S-rich aromatic fractions was characterised using a HP 6890 GC interfaced to an Agilent 5975 mass selective detector (MSD). The GC was fitted with a DB-5MS capillary column (60 m × 0.25 mm i.d. × 0.25 μm film thickness). Helium carrier gas was used at a constant flow rate of 1.3 mL/min and the GC oven temperature was programmed from an initial 40 °C (held 2 min) to 325 °C (held for 30 min) at a rate of 3 °C/min. The MSD was operated at a source temperature of 230 °C. Full scan (*m/z* 30–530 Da) 70 eV mass spectra were acquired at a rate of ~ 4 scans per second.

Parent and alkyl DBT products were identified based on correlation of the mass spectral and GC analyses to laboratory standards and published data (Asif et al., 2009; Grotheer et al., 2017). Quantification of DBT (184 Da) and methyl DBT (198 Da) compounds were determined by correlation of parent ion peak areas to an external calibration curve established with several DBT standards of different concentration.

3.3. Compound Specific Sulfur Isotope Analysis

The $\delta^{34}S$ values of DBTs in the S rich aromatic fraction (III) were analysed using an Agilent 6890 GC interfaced to a Thermo Neptune Plus multi-collector inductively coupled plasma mass spectrometer (MC-ICP-MS; Greenwood et al., 2014). The S-analytes were separated on the GC with a DB-5 MS column (30 m × 0.25 mm i.d. × 0.1 μm film thickness). The GC oven was heated from 100 °C (held for 0.5 min) to an end temperature of 300 °C (held for 15 min) at a rate of 8 °C/min. Argon gas

for the ICP torch was pre-heated to assist the transfer of analytes from the GC. An SF_6 gas standard of known $\delta^{34}S$ value was used for tuning and calibration of the MC-ICP-MS. Two pulses of SF_6 were included at both the start and end of all GC-MC-ICP-MS analyses to internally calibrate $\delta^{34}S$ measurements. $\delta^{34}S$ results were reported as permil (‰) relative to the international sulfur isotope standard Vienna Canyon Diablo Troilite (VCDT).

A $\delta^{34}S$ precision of < 0.2 ‰ is typically for OSCs with ≥ 80 pmol sulfur (Greenwood et al., 2014) and confirmed by daily analyses of a mixture comprising four authentic S-compounds (benzothiophene, dodecanthiol, dibenzothiophene and octadecanethiol). The duplicate analysis of the Meishan samples mostly gave $\delta^{34}S_{OSC}$ values with a standard variance < 0.5 ‰.

3.4. Isolation, quantification and isotopic analysis of bulk S fractions

Sedimentary total reducible inorganic sulfur (TRIS) fraction – essentially considered to consist of pyrite (FeS_2) – was separated from dry sediment powders according to a single-step hot acidic Cr(II) distillation (Fossing and Jørgensen, 1989). Generated H_2S was trapped in a Zn acetate solution and measured spectrophotometrically (Specord 40, Analytical Jena). Results were used to calculate the TRIS content in wt% of dry sample (% dwt). For stable isotope measurements, ZnS was transferred into Ag_2S using an $AgNO_3$ solution, washed and dried. The residue from Cr(II) distillation was considered as being representative of kerogen (Passier et al., 1999). Combustion-isotope ratio monitoring mass spectrometry (C-irmMS) analysis of Ag_2S samples and washed and dried residues from the Cr(II) distillation (i.e., KerS) were conducted by combustion in a Thermo Flash 2000 elemental analyser, connected to a Thermo Finnigan MAT 253 gas mass spectrometer *via* a Thermo Conflow IV interface.

3.5. Fe Speciation

The pyrite-associated iron fraction (Fe_{Py}) was calculated assuming ideal FeS_2 stoichiometry from the analytical TRIS amounts. Total iron (Fe_T) was measured using ICP-OES (Thermo Icap 6300 DUO) after complete acid digestion in a pressure digestion system PDS-6 (Loftfield Analytical Solutions; Heinrichs et al., 1986; Kowalski et al., 2012). The remaining reactive sedimentary iron was extracted with 1 M HCl (Fe_{HCl}) or buffered sodium dithonite solution (Fe_D; Canfield, 1989) and measured spectrophotometrically (Specord 40, Analytical Jena). The highly reactive iron fraction (Fe_{HR}) was calculated as the sum of dominating Fe_{Py} and Fe_{HCl} or Fe_D.

4. Results

Geochemical parameters measured from the Meishan-1 sediments including $\delta^{34}S$ (‰) and content (% wt) of TRIS, KerS and DBT as well as Fe phase ratios are given in Table 1. The $\delta^{34}S_{TRIS}$, $\delta^{34}S_{KerS}$ and $\delta^{34}S_{DBT}$ profiles of the Meishan-1 section studied are displayed in Fig. 1 (Fig. 1A-C show $\delta^{34}S$ profile of whole section; Fig. 1G-I expands $\delta^{34}S$ profile of beds 22–34); and the abundance profiles of TRIS, KerS as well as of the TRIS/(TRIS + KerS) ratio and TOC are given in Fig. 2.

$\delta^{34}S_{TRIS}$ was −36.5 ‰ in the deepest sample (153.95 m), then relatively stable at ~ -27 ‰ (±2 ‰) through most of the Late Permian (beds 12–21; Fig. 1A). A large fluctuation in $\delta^{34}S_{TRIS}$ was evident closer to the extinction transition, comprising increasing values (~ +15 ‰) through bed 22 to a maximum value of −13.4 ‰ in the lower Bed 24 sample, then receded in bed 26 to values (−25 to −30 ‰) similar to those in the deeper Late Permian samples (Fig. 1G). The Early Triassic sample (bed 34) showed a further $\delta^{34}S_{TRIS}$ decrease to −37 ‰.

Interestingly $\delta^{34}S_{KerS}$ was relatively stable at approx. −16 ‰ below 140 m (beds 7–14), then increased moderately to −11 ‰ at the bottom of bed 22 where it generally remained through the remaining P-T transition (Fig. 1B). It did not fluctuate in value through bed 22–24 like

Table 1
Content and isotopic data of S-phases; iron speciation data; and isorenieratane and C_{14}-C_{27} arylisoprenoid concentrations (from Grice et al., 2005*) of Meishan-1 sediments.

Sample #	Depth [m]	Bed #	TOC [wt% Sed.]	TRIS [% dwt]	$\delta^{34}S_{TRIS}$ [‰]	KerS [% Cr^{2+} residue]	$\delta^{34}S_{KerS}$ [‰]	DBT [µg/g TOC]	$\delta^{34}S_{DBT}$ [‰]	ΣmDBT [µg/g TOC]	$\delta^{34}S_{\Sigma mDBT}$ [‰]	TRIS/ (TRIS + KerS)	IsoR* (µg/g TOC)	AryI* (µg/g TOC)	Fe_{HR}/Fe_T	Fe_{Py}/Fe_{HR}	Redox milieu (after Li et al., 2010)
1	102.59	34	0.61	1.02	−36.4	0.01	−20.9	2.4	--	3.2	--	0.99	0.00	29.4	0.26	0.87	oxic
2	106.52	26	0.81	1.54	−25.3	0.04	−18.6	18.4	−20.5	67.3	−17.4	0.97	0.66	343.0	0.39	0.95	oxic/euxinic
3	106.56	26	0.72	1.36	−27.6	0.02	−15.8	9.1	−20.3	35.0	−21.5	0.99	0.00	150.1	0.39	0.95	oxic/euxinic
4	106.74	24	0.67	0.22	−15.7	0.07	−8.7	26.1	−19.4	107.2	−20.3	0.76	0.83	19.39	0.54	0.56	ferruginous
5	107.10	24	0.30	0.10	−13.4	0.37	−10.6	9.6	−23.6	31.1	−24.4	0.21	55.83	1432.9	0.64	0.65	ferruginous
6	110.15	22	0.50	0.09	−16.9	0.20	−10.7	5.4	−20.5	15.7	−19.9	0.31	24.39	126.49	0.53	0.80	euxinic/ferruginous
7	111.04	22	1.27	0.16	−28.4	0.10	−11	5.8	−16.9	25.5	−19.9	0.62	0.00	106.85	0.42	0.90	euxinic
8	125.46	15–21	0.54	0.07	−26.1	0.23	−13.6	41.1	−24.4	303.2	−22.5	0.23	0.02	38.17	0.42	0.97	euxinic
9	140.01	12–14	0.32	0.03	−27.2	0.91	−16.2	34.2	−28.8	145.5	−28.5	0.03	97.44	2723.0	0.48	0.94	euxinic
10	148.50	12–14	0.31	0.02	−24.6	0.59	−16.2	24.4	−22.7	139.0	−22.8	0.03	59.93	1339.2	0.36	0.92	oxic
11	153.95	7–11	1.22	0.18	−36.5	0.27	−16.4	64.7	−21.8	412.7	−22.9	0.40	0.76	128.7	0.46	0.95	euxinic

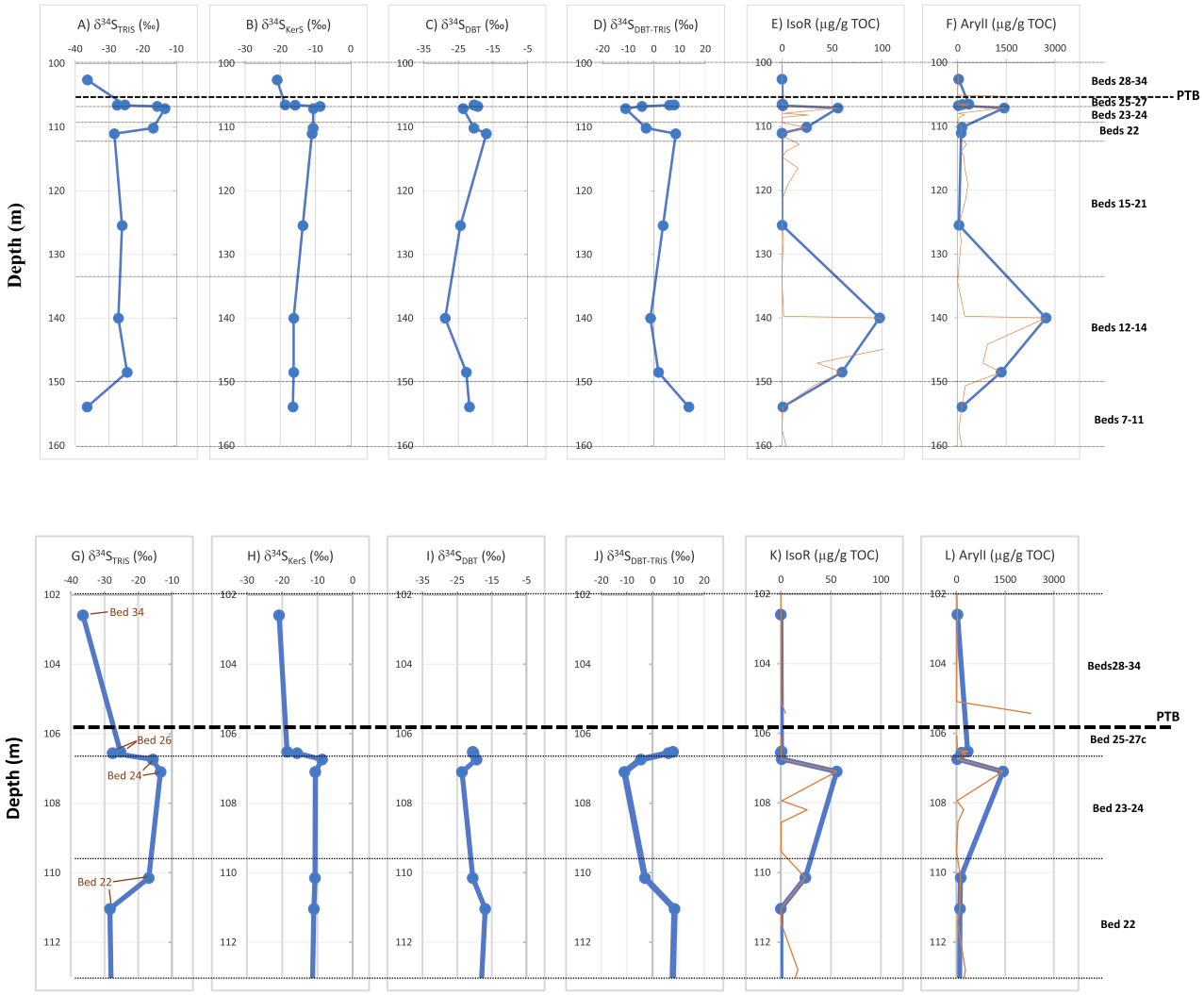

Fig. 1. Meishan-1 $\delta^{34}S$ profiles of (A) TRIS; (B) KerS; (C) DBT; (D) DBT-TRIS; and abundance profile of the euxinic/anoxic biomarkers (E) isorenieratane (IsoR); (F) $\Sigma(C_{14}\text{-}C_{27})$ arylisoprenoids (ArylI). E-F data from Grice et al. (2005) – included for correlation of water column redox with the S-isotopic data: blue data points/profile correspond to samples of present study; orange data points/profile are from full sample suite of Grice et al. (2005). (G-L) showed zoomed bed 22–34 regions of (A-F). (For interpretation of the references to colour in this figure legend, the reader is referred to the web version of this article.)

observed for $\delta^{34}S_{TRIS}$, but did reflect a notable ^{34}S depletion ($\delta^{34}S_{KerS}$ = -19 ‰) in upper bed 26 just before the PTB (Fig. 1H). The Early Triassic bed 34 sample showed a further ^{34}S depletion with $\delta^{34}S_{KerS}$ = -21 ‰, which was similar to the $\delta^{34}S_{TRIS}$ value measured in this youngest sample.

Individual OSCs for which $\delta^{34}S$ values were measured were DBT and mDBT – the three separate GC peaks of latter (4-methyl, co-eluting 2&3-methyl and 1-methyl) were co-integrated and $\delta^{34}S$ reported as ΣmDBT. No other OSCs were detected with sufficient abundance (≥80 pmol S per compound; Greenwood et al., 2014) for reliable $\delta^{34}S$ measurement. $\delta^{34}S$ values of co-eval DBT and ΣmDBT were generally similar (Table 1) so for brevity just $\delta^{34}S_{DBT}$ will be discussed here forth. Through the deeper Late Permian section (bed 7–22; Fig. 1C) $\delta^{34}S_{DBT}$ ranged between a low of −29 ‰ (140.01 m) and high −17 ‰ (111.04 m/bed 22). Through bed 22–24, coincident with the fluctuation in $\delta^{34}S_{TRIS}$ values, $\delta^{34}S_{DBT}$ showed a small decrease to −24 ‰ (bed 24–107.1 m) then similar magnitude rebound to −19 ‰ (bed 24–106.74 m; Fig. 1I). It remained relatively stable through bed 26 (−20 ‰). A low DBT concentration (2.4 µg/g) unfortunately precluded a $\delta^{34}S$ measurement of the Early Triassic sample (102.6 m/bed 34).

5. Discussion

5.1. Sulfur Biogeochemistry and $\delta^{34}S$

The sulfur (S) of sulfide minerals and organic sediments is largely sourced from the reduction of seawater SO_4^{2-} by sulfate reducing bacteria (SRB). The end product of sulfate reduction is H_2S which can subsequently react with reactive metal ions (e.g., Fe^{2+}, Mn^{2+}) or organic matter depending on their availability. Pyrite (FeS_2) formation is the kinetically favored process (Hartgers et al., 1997). Organic sulfurisation proceeds via the transformation of H_2S to a range of intermediate oxidation compounds with different S-valences (e.g., HS^-, S_x^-, S^0, $S_2O_3^{2-}$, SO_3^{2-}), though these reactive species are also susceptible to other transformation processes (i.e., bacterial reduction to H_2S; mineral precipitation, e.g., FeS; S^0 disproportionation to H_2S and SO_4^{2-}; Canfield and Thamdrup, 1994; Canfield, 2001).

A $\delta^{34}S$ based model of the sulfur cycle of a marine sedimentary system is shown in Fig. 3. The microbial reduction of SO_4^{2-} (blue arrow, Fig. 3) has a strong kinetic bias against ^{34}S and imparts a first order control on the $\delta^{34}S$ values of environmental samples (Canfield, 2001). The magnitude of S-isotopic fractionation due to microbial (dissimilatory) sulfate reduction has been measured to vary widely with SRB

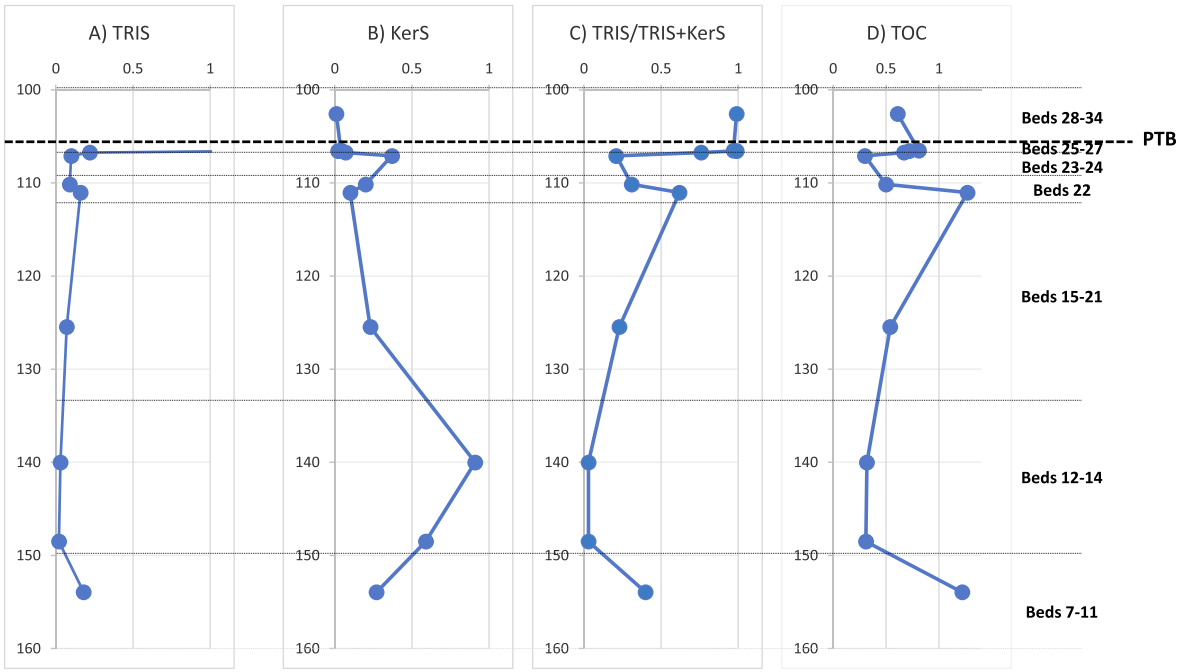

Fig. 2. Meishan-1 abundance profile of (A) TRIS; (B) KerS; (C) TRIS/(TRIS + KerS); and (D) TOC.

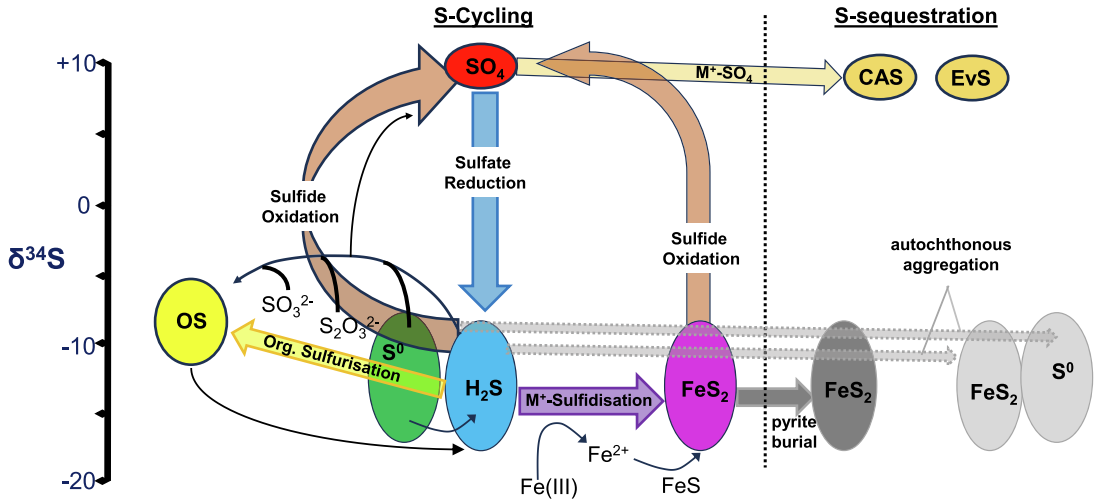

Fig. 3. Major biotic and abiotic S transformation pathways and general $\delta^{34}S$ relationships of the S-cycle of P-T marine sediments. Major processes include sulfate reduction (blue arrow; Nb. $\delta^{34}S$ of seawater sulfate source at P-T ≈ +10 ‰), sulfide mineralisation (purple), organic sulfurisation (yellow) and sulfide oxidation (brown). Pathways which may sequester S from the cycle include carbonate associated (CAS) and evaporative (EvS) sulfate formation (orange), pyrite burial (dark grey) or autochthonous S-aggregation (light grey). Black arrows provide further secondary detail of the interconnectivity between the major S-phases and several important intermediate sulfur species – including elemental sulfur (highlighted green) which can directly link the sulfate-sulfide-sulfurised reservoirs of S. (For interpretation of the references to colour in this figure legend, the reader is referred to the web version of this article.)

species and environment, ranging from just 2 ‰ (Detmers et al., 2001) to as large as 72 ‰ (Wortmann et al., 2001), but generally is in a narrower range of 20 ‰ to 45 ‰ (Hartmann and Nielsen, 2012; Goldhaber and Kaplan, 1980; Chambers and Trudinger, 1979; Habicht and Canfield, 1997; Brüchert et al., 2001). A quite consistent fractionation of approx. 20 ‰ was suggested for microbial sulfate reduction based on a comparison of the $\delta^{34}S$ values of petroleum samples (i.e., whole oils) spanning a wide range of phanerozoic ages and coeval seawater SO_4^{2-} inferred from $\delta^{34}S$ measurements of evaporative or carbonate associated sulfate (Engel and Zumberge, 2007).

Secondary $\delta^{34}S$ impacts on the main S-phases (i.e., H_2S, SO_4^{2-}) are imparted from other S cycling stages and potentially also gradual sequestration of some parts. The transformation of H_2S to FeS_2 (i.e., pyritization; purple arrow, Fig. 3) occurs with negligible S-isotopic fractionation (<1 ‰; Price and Shieh, 1979; Canfield, 2001). Comparatively, the diagenetic reaction of functionalised or reactive organic molecules with reduced sulfur intermediates (yellow arrow, Fig. 3) to form organic sulfur usually occurs with a modest ^{34}S enrichment leading to an increase in the $\delta^{34}S_{OS}$ of a few ‰ (cf., $\delta^{34}S_{H2S}$; Anderson and Pratt, 1995; Amrani and Aizenshtat, 2004a, 2004b). Oxidizing bacteria can convert sulfides back to sulfate (brown arrows, Fig. 3), adding ^{34}S depleted S back to the previously ^{34}S enriched residual SO_4^{2-} pool, potentially reversing most of the isotopic bias introduced by the initial microbial sulfate reduction. Furthermore, S^0 may be utilised by autotrophic sulfur disproportionating bacteria (SDB) and partially converted in an equilibrium reaction to sulfate and sulfide, experiments with

enrichment cultures of SDB showing the $\delta^{34}S$ value of the produced sulfate approx. + 14 ‰ higher and sulfide −8 ‰ lower, respectively, than that of elemental S (Canfield and Thamdrup, 1994).

Various processes might also remove sulfur from the cycling system. One common event is the burial of pyrite, impacting the sulfide pool available to sulfide oxidisers or potentially the stochiometric buffering support for the SDB conversion of S^0. S might also be removed via direct microbial (e.g., biofilm) aggregation of the secondary products of sulfate reduction (e.g., S^0, FeS_2; Raven et al., 2016), with the autocthonous sequestration of ^{34}S depleted S having a ^{34}S enrichment effect on the continuing S-cycles.

Other environmental factors which can contribute to large $\delta^{34}S$ differences between the main S-phases include a strong redox dependance of biotic and abiotic sulfurisation processes. The magnitude of S-isotopic fractionation may be amplified with repeated reduction–oxidation cycling as has been credited for the very large $\delta^{34}S$ fractionations (40–70 ‰) determined between seawater SO_4^{2-} and the sulfides in modern anoxic waters like the Black Sea (Fry et al., 1991; Canfield and Thamdrup, 1994). The mixing of S-phases involved in different cycles may also moderate the full S-isotopic fractionation effect of particular disproportionation or fractionation processes.

5.2. Seawater $\delta^{34}S$ of Late Permian and Early Triassic

Several paleo-reconstructions of seawater $\delta^{34}S_{SO4}$ values have been established from isotopic measurements of evaporative sulfates, pyrites and CAS, including through the Permian and Triassic periods (e.g., Newton et al., 2004; Kaiho et al., 2006a; Bernasconi et al., 2017). These studies have generally shown $\delta^{34}S_{SO4}$ to decrease in the very late Permian to Phanerozoic minimums typically close to + 10 ‰ near the PTB, before returning to more ^{34}S enriched values through the Early Triassic. A high-resolution reconstruction (Bernasconi et al., 2017) of seawater $\delta^{34}S$ from gypsum and anhydrite measurements of several studies (e.g., Worden et al., 1997; Insalaco et al., 2006; Bernasconi et al., 2017) indicated a small Late Permian (Lopingian) decrease (+11 ‰ to + 8 ‰) adjacent to the PTB, followed by a sharp increase to more than + 30 ‰ in the Early Triassic before a more gradual decline to approx. + 17 ‰ through the Late Triassic. A more pronounced Late Permian decrease (−30 ‰) in CAS measured $\delta^{34}S_{SO4}$ values to a relatively low minimum of 0 ‰ was reported in a previous study of Meishan outcrop sediments (bed 24e to bed 29; Kaiho et al., 2006a).

The Late Permian ^{34}S depletion of seawater SO_4^{2-} was caused by greater mixing of the prevailing stratified and anoxic ocean (Nb., supported by co-incident ^{18}O depletion of CAS; Newton et al., 2004), with an increase in reactive iron and sequestration of S as pyrite contributing to an amplification of $\delta^{34}S_{SO4}$ dynamics. Re-oxidation of BSR reduced H_2S (Newton et al., 2004) and meteorite impact (Kaiho et al., 2001, 2006b) have both been suggested as potential triggers of major ocean turbulence. Substantial pyrite burial would have significantly decreased the marine sulfate reservoir, potentially aiding the large $\delta^{34}S$ variations measured through the P-T transition (Newton et al., 2004, Hay et al., 2006) which were far more dynamic than the long residence times (~10–20 Myr) and slow $\delta^{34}S_{SO4}$ flux (1.1 ‰ change per Myr) of our modern oceans (Algeo et al., 2015).

5.3. $\delta^{34}S_{TRIS}$ dynamics of Meishan P-T

The $\delta^{34}S_{TRIS}$ values of −27 ± 2 ‰ through most of the late Permian (beds 12–21) were interrupted in the P-T transition (beds 22–24; Fig. 1G) with an apparent ^{34}S enrichment phase to reach a maximum −13 ‰ before returning to approx. −27 ‰ just prior to the PTB (beds 24–26). The $\delta^{34}S_{TRIS}$ increase interval coincided with elevated abundances of the green sulfur bacterial biomarkers isorenieratane (Fig. 1E and K) and arylisoprenoids (Fig. 1F and 1L; Grice et al., 2005) indicative of photic zone euxinic oceans.

The $\delta^{34}S_{TRIS/pyrite}$ values of a P-T section spanned by Tenjinmaru rocks (Chichibu Terrane, Japan; Kajiwara et al., 1994) showed a similar trend, with Late Permian values mostly around −25 ‰ becoming sharply higher in the extinction event to a maximum value of −7 ‰ near the PTB. The Early Triassic rocks of this section also showed $\delta^{34}S_{TRIS}$ values extending to less than −40 ‰, indicative of greater ^{34}S depletion (Kajiwara et al., 1994).

Further, the presently reported $\delta^{34}S_{TRIS}$ profile is generally consistent with previous measurement of $\delta^{34}S_{SO4}$ (CAS) and $\delta^{34}S_{py}$ data from Meishan-1 (Kaiho et al., 2001, 2012; Riccardi et al., 2006; Song et al., 2014). Data through bed 22–24 reported by Riccardi et al. (2006) comprised $\delta^{34}S_{SO4}$ values mostly near 0 ‰ from bed 22 to near top of bed 23; then fluctuated between 0 ‰ to + 25 ‰ in bed 24 (most values at the higher end); with bed 24 $\delta^{34}S_{py}$ values between −25 ‰ and −12 ‰ (Nb., −25 ‰ to −37 ‰ < $\delta^{34}S_{SO4}$).

5.4. $\delta^{34}S_{KerS}$ dynamics of Meishan P-T

The Late Permian $\delta^{34}S_{kerS}$ profile was relatively stable (approx. −11 ‰) through most of the P-T transition (Fig. 1B and H; Table 1), including in beds 22 – 24 when $\delta^{34}S_{TRIS}$ sharply increased (~ +15 ‰). $\delta^{34}S_{kerS}$ decreased, indicative of more ^{34}S depletion, in bed 26 and more so in the Early Triassic which is consistent with the relatively low $\delta^{34}S_{SO4}$ and $\delta^{34}S_{TRIS}$ values of this sample. $\delta^{34}S_{KerS}$ were mostly > 10 ‰ than co-eval $\delta^{34}S_{TRIS}$ through the whole of Meishan-1, typical of the preferential kinetic reaction of the ^{34}S depleted reduced sulfur pool (i.e., H_2S) with iron to form pyrite with negligible S isotopic bias (Price and Shieh, 1979; Canfield, 2001), and secondary organic sulfurisation of reduced or intermediate S with a small enrichment of ^{34}S (Anderson and Pratt, 1995; Amrani and Aizenshtat, 2004a, 2004b), under normal equilibrium conditions.

The disconnect between $\delta^{34}S_{kerS}$ values and the more dynamic $\delta^{34}S_{TRIS}$ behavior (and other biochemical indicators) through the extinction transition indicates KerS has a reduced isotopic sensitivity to the extinction causes. Fe speciation data of the Meishan samples (Fig. 4A-C), indicated the bed 22–24 samples in which the high $\delta^{34}S_{TRIS}$ values were recorded had Fepy/FeT values < 0.8 indicative of ferruginous conditions, and distinct from the other Meishan 1 samples (Fepy/FeT values > 0.8). Furthermore, bed 22–24 showed a decrease in the abundance of TRIS (Fig. 2A) which in an Fe^{2+} rich environment implies a limitation of reduced S. In S limited systems there is less opportunity to preferentially utilise the lighter isotope, often resulting in higher $\delta^{34}S$ values which was evident in the bed 22–24 enrichment excursion of $\delta^{34}S_{TRIS}$ (Fig. 1G). The content changes in TRIS and KerS are amplified by the TRIS/(TRIS + KerS) ratio which is a sensitive redox parameter and likely influenced in Meishan by the fluctuating euxinic/ferroginous intervals.

The insensitivity of $\delta^{34}S_{KerS}$ to these redox dynamics may be due to the large sulfurisation collective represented by this fraction. S can be incorporated into kerogen from several different sources and via multiple pathways, including directly within the molecular lattice (intramolecular S) or as oxidized sulfur bridges (e.g. S_x^{2-}) between discrete organic units (intermolecular S) (Amrani, 2014).

5.5. $\delta^{34}S_{DBT}$ dynamics of Meishan P-T

The $\delta^{34}S_{DBT}$ values of the Meishan sediments ranged from −29 ‰ to −17 ‰ and were significantly lower than $\delta^{34}S_{KerS}$ (i.e., by as much as −15 ‰). In the late Permian they had similar values and trajectory to co-eval $\delta^{34}S_{TRIS}$, until a decrease in beds 22–24 (−17 ‰ to −24 ‰) which was inverse to the enrichment excursion observed for $\delta^{34}S_{TRIS}$. The isotopic digression between $\delta^{34}S_{TRIS}$ and $\delta^{34}S_{DBT}$, amplified by the $\Delta\delta^{34}S_{DBT\text{-}TRIS}$ parameter profiled in Fig. 1D and 1J, suggests a coincident response to the redox changes (high Fe^{2+} availability) in the water column.

The negative $\Delta\delta^{34}S_{DBT\text{-}TRIS}$ values of the bed 22–24 excursion identifies DBTs to be more depleted than TRIS, which is atypical of the

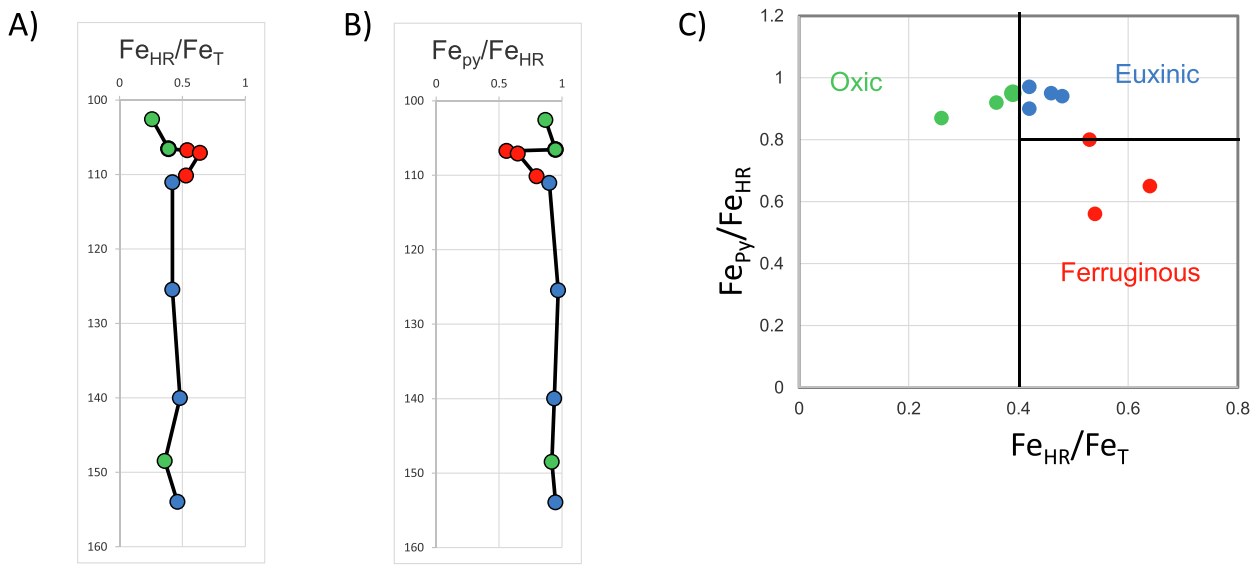

Fig. 4. Iron speciation profiles of Meishan-1 (A) highly reactive Fe relative to total Fe (Fe_{HR}/Fe_T); (B) pyrite Fe relative to highly reactive Fe (Fe_{py}/Fe_{HR}); and (C) Cross plot of Fe_{PY}/Fe_{HR} versus Fe_{HR}/Fe_T reflecting the redox conditions of the water column during deposition (Li et al., 2010). A-C data points shaded green = oxic deposition; blue = euxinic deposition; and red = ferruginous deposition. (For interpretation of the references to colour in this figure legend, the reader is referred to the web version of this article.)

normal kinetic bias of pyrite formation over organic sulfurisation. Organic sulfur could potentially become more ^{34}S depleted than pyrite with multiple sulfate reduction-sulfide oxidation cycles in an organic matter-rich, iron-limited system, such that Fe^{2+} is consumed prior to the exhaustion of organic sulfurisation which continues to utilise a gradually ^{34}S depleted reduced S pool. This scenario would seem unlikely for Meishan-1 given the negative $\Delta\delta^{34}S_{DBT\text{-}TRIS}$ values coincide with ferruginous deposition. The DBTs might, however, be syngenetically produced from an open SO_4^{2-} system within the water column maintained over a relatively prolonged ferruginous period, whilst the pyrite is diagenetically produced below the sediment–water interface from the reduced S of slowly diffusing porewater SO_4^{2-} that becomes isotopically enriched with depth (Shawar et al., 2018, 2020).

Other plausible explanations for the occurrence of OSCs that are ^{34}S depleted compared to pyrite include i) irreversible incorporation of S_x^- anions into organic sulfur compounds with a kinetic isotope effect – although this mechanism has been observed to produce OSCs only a few ‰ lighter than pyrite (Amrani et al., 2008), so may not account for the up to 15 ‰ discrepancy measured in Meishan sediments; or ii) an organic sulfurisation pathway that is more reactive than Fe to S_x^- reactants (Shawar et al., 2020).

Organic reactants involved in subsurface sulfurisation reactions yielding products such as DBTs are not well understood (Amrani et al., 2014). DBTs have been produced in the laboratory by reaction of hydrocarbon compounds such as petroleum *n*-alkanes (Kowalewski et al., 2010; Nguyen et al., 2013) and biphenyls (Asif et al., 2009) with reduced S (e.g. H_2S, S^0). The DBTs might also be later diagenetic products of primary OSCs (e.,g alkyl thiophenes, triterpenoid thiane and highly branched isoprenoid thiolanes) produced by the interaction of inorganic sulfur species with functionalised lipids in organic sediments (Brassell et al., 1986; Deshmukh et al., 2001). Several such primary OSCs were measured to have low $\delta^{34}S$ values compared to pyrite ($\Delta\delta^{34}S_{OSC\text{-}pyrite}$ up to −10 ‰) and more so kerogen ($\Delta\delta^{34}S_{OSC\text{-}Ker}$ up to −20 ‰) in sediments from the Cariaco Basin, a modern anoxic, sulfidic rich basin north of Venezuala (Raven et al., 2015). Different organic sulfurisation pathways were suggested as a potential reason for this isotopic discrepancy. Bisulfide (HS-) reactants were preferred over polysulfides (S_x^-) as a likely source of the ^{34}S depleted OCS on the bases of energetics and an ensuing kinetic isotope effect implied from the respective $\delta^{34}S$ versus depth profiles of the different S-species measured in the Cariaco Basin sediments (Raven et al., 2015).

Variations in molecular structure (e.g., functional groups) might also influence the reactivity and S isotope fractionation of organic sulfurisation pathways (Amrani and Aizenshtat,2004a,b; Amrani et al., 2008; Amrani, 2014). The $\delta^{34}S$ of OSCs co-occurring in immature sediments can span a wide range of values ($\Delta\delta^{34}S$ of different OSCs > 30 ‰; Werne et al., 2008; Raven et al., 2015, Shawar et al., 2020). The $\Delta\delta^{34}S$ between OSCs was observed to increase with pyrite content (and presumed availability of Fe^{2+}), suggesting organic sulfurisation was competing with pyritization for the available S, with slower sulfurisation reactions having to utilise a residual and isotopically heavier reduced S pool (Shawar et al., 2020).

Specifics OSCs or classes of compounds may be representative of specific sulfurisation processes, reaction rates or spatial dynamics such as micro-environments (e.g. microbial aggregates, biofilms) which can influence the $\delta^{34}S$ of porewater sulfides and pyrite (Raven et al., 2016). The temporal and spatial controls on S-cycling processes may be less resolvable from the entirety of the kerogen sulfur which is typically representative of a combination of sulfurisation processes contributing diverse $\delta^{34}S$ values. Sulfurisation reactions producing OSCs (e.g., DBTs) are also likely to occur much more rapidly than the time it takes to develop or infiltrate the 3-dimensional covalent lattice of kerogen – thus may be less vulnerable to secondary processes and fractionations which can dissipate $\delta^{34}S$ signatures. The relatively small S-content of individual OSCs might also aid their responsiveness to biochemical dynamics such as the $\delta^{34}S$ character of incident BSR (Raven et al., 2016). The bed 22 abundances of DBTs (<6 μg/g) were much lower than the deeper Permian sediments (>24 μg/g) which could make them more sensitivity to changes in the reactivity or isotopic character of incident S supplies.

6. Conclusions

The $\delta^{34}S$ of individual OSCs, likely representative of particular organic S-moieties or sulfurisation processes, can complement the more traditional organic sulfur isotopic analysis of kerogen. The $\delta^{34}S$ of DBTs and reduced inorganic S in Meishan-1 showed opposing isotopic excursions in a transition interval just prior to the PTB. The inverted DBT and TRIS isotopic trends were driven by fluctuating euxinic and ferruginous ocean conditions and resulted in negative $\Delta\delta^{34}S_{DBT\text{-}TRIS}$ values indicating greater ^{34}S discrimination by organic sulfur than pyrite

formation which is usually kinetically favored. The $\delta^{34}S_{DBT}$ deviation was not reflected by $\delta^{34}S_{KerS}$, however, highlighting the enhanced sensitivity of individual organic S compounds to certain S-biochemical fluxes and the biochemical clarity that the $\delta^{34}S$ values of OSCs can provide. The $\delta^{34}S$ values of bulk organic fractions like kerogen, on which previous organic sulfurisation evaluations have been traditionally based, represent an average value of many different sulfurisation processes.

Sulfurisation controls which might account for the negative $\Delta\delta^{34}S_{DBT\text{-}TRIS}$ values measured during the extinction interval include an organic substrate with an unusually higher reaction affinity for S_x^{2-} than Fe^{2+}; or an organic sufurisation pathway with an irreversible kinetic isotope effect. Spatial or temporal differences in the formation of different S-species might also be a factor. Preferential organic sulfurisation in a ferruginous (Fe^{2+} rich) water column point to an open SO_4^{2-} system, but the isotopically light DBTs could preferentially form in the water column (i.e., syngenetic formation) whereas pyrite may mostly derive from sedimentary (diagenetic) utilisation of H_2S from the SRB of diffused and progressively ^{34}S enriched SO_4^{2-}. The actual impact of some of these controls could be explored further with laboratory simulated experiments and incorporation of compound specific $\delta^{34}S$ analysis to resolve different organic sulfurisation processes.

The S-biogeochemistry dynamics of the P-T transition provided here by $\delta^{34}S$ measurement and evaluation of reduced and organic S phases of Meishan-1 sediments demonstrates how they can complement traditional sulfate-based characterisation of S-cycles throughout Earth's history. Further application of this approach could help to further resolve the S-fluxes of other major mass extinction events.

CRediT authorship contribution statement

Paul F. Greenwood: Writing – review & editing, Writing – original draft, Supervision, Formal analysis, Conceptualization. **Hendrik Grotheer:** Writing – review & editing, Writing – original draft, Formal analysis, Conceptualization. **Michael E. Böttcher:** Data analysis - bulk $\delta^{34}S$ and Fe speciation analyses, Writing and Reviewing Manuscript. **Kliti Grice:** Conceptualization, Supervision, Sample Provision, Writing and Reviewing Manuscript.

Declaration of competing interest

The authors declare that they have no known competing financial interests or personal relationships that could have appeared to influence the work reported in this paper.

Data availability

All data generated in this study or used in the Figures are included in Table 1.

Acknowledgments

This study was conducted as part of the CSIRO Flagship Collaboration Fund Cluster for Organic Geochemistry of Mineral Systems. HG thanks CSIRO and Curtin University (scholarships), KG the ARC (DP150102235; FL210100103) and MEB the Leibniz IOW for funding support. Alex I. Holman, Geoff Chidlow, Peter Hopper (all Curtin University) and Iris Schmiedinger and Anne Köhler (all IOW) provided analytical support. Roger E. Summons (MIT) and Cao Changqun (NIGPAS) are thanked for providing the Meishan-1 samples. We thank two anonymous journal reviewers for their constructive advice which improved earlier versions of this manuscript.

References

Algeo, T.J., Luo, G.M., Song, H.Y., Lyons, T.W., Canfield, D.E., 2015. Reconstruction of secular variation in seawater sulfate concentrations. Biogeosciences 12, 2131–2151.
Amrani, A., 2014. Organosulfur compounds: molecular and isotopic evolution from Biota to Oil and Gas. Annual Reviews of Earth and Planetary Science. 42, 733–768.
Amrani, A., Aizenshtat, Z., 2004a. Mechanisms of sulfur introduction chemically controlled: δ34S imprint. Organic Geochemistry 35, 1319–1336.
Amrani, A., Aizenshtat, Z., 2004b. Reaction of polysulfide anions with α,β unsaturated isoprenoid aldehydes in aquatic media: Simulation of oceanic conditions. Organic Geochemistry 35, 909–921.
Amrani, A., Ma, Q., Ahmad, W.S., Aizenshtat, Z., Tang, Y., 2008. Sulfur isotope fractionation during incorporation of sulfur nucleophiles into organic compounds. Chemical Communications 22, 1356–1358.
Amrani, A., Sessions, A.L., Adkins, J.F., 2009. Compound-specific $\delta^{34}S$ analysis of volatile organics by coupled GC/multicollector-ICPMS. Analytical Chemistry 81, 9027–9034.
Anderson, T.F., Pratt, L.M., 1995. Ch. 21 Isotopic Evidence for the Origin of Organic Sulfur and Elemental Sulfur in Marine Sediments. In: Vairavamurthy, M.A., Schoonen., M.A.A., Eglinton, T.I., Luther III, G.W., Manowitz, B. (Eds.), Geochemical Transformations of Sedimentary Sulfur (ACS Symposium Series 612, 1995). ACS publications, Washington, DC, pp. 378–396.
Asif, M., Alexander, R., Fazeelat, T., Pierce, K., 2009. Geosynthesis of dibenzothiophene and alkyl dibenzothiophenes in crude oils and sediments by carbon catalysis. Organic Geochemistry 40, 895–901.
Benton, M.J., Twitchett, R.J., 2003. How to kill (almost) all life: the end-Permian extinction event. Trends in Ecology & Evolution 18, 358–365.
Bernasconi, S.M., Meier, I., Wohlwend, S., Brack, P., Hochuli, P.A., Bläsi, H., Wortmann, U.G., Ramseyer, K.R., 2017. An evaporative-based high-resolution sulfur isotope record of late Permian and Triassic seawater sulfate. Geochimica et Cosmochimica Acta 204, 331–349.
Berner, R.A., Raiswell, R., 1983. Burial of organic carbon and pyrite sulfur in sediments over phanerozoic time: a new theory. Geochimica et Cosmochimica Acta 47, 855–862.
Bowring, S.A., Erwin, D.H., Jin, Y.G., Martin, M.W., Davidek, K., Wang, W., 1998. U/Pb Zircon Geochronology and Tempo of the End-Permian Mass Extinction. Science 280, 1039–1045.
Bowring, S.A., Erwin, D.H., Isozaki, Y., 1999. The tempo of mass extinction and recovery: the end-Permian example. Proceedings of National Acadamey of Sciences. 96, 8827–8828.
Brassell, S.C., Lewis, C.A., De Leeuw, J.W., de Lange, F., Sinninghe Damsté, J.S., 1986. Isoprenoid thiophenes: novel products of sediment diagenesis? Nature 320, 160–162.
Brüchert, V., Knoblauch, C., Jorgensen, B.B., 2001. Controls on stable sulfur isotope fractionation during bacterial sulfate reduction in Arctic sediments. Geochimica et Cosmochimica Acta 65, 763–776.
Canfield, D.E., 1989. Reactive iron in marine sediments. Geochimica et Cosmochimica Acta. 53, 619–632.
Canfield, D.E., 2001. Biogeochemistry of sulfur isotopes. Reviews in Mineralogy and Geochemistry 43, 607–636.
Canfield, D.E., Teske, A., 1996. Late Proterozoic rise in atmospheric oxygen concentration inferred from phylogenetic and sulphur-isotope studies. Nature 382, 127–132.
Canfield, D.E., Thamdrup, B., 1994. The production of ^{34}S-depleted sulfide during bacterial disproportionation of elemental sulfur. Science 266, 1973–1975.
Cao, C., Love, G.D., Hays, L.E., Wang, W., Shen, S., Summons, R.E., 2009. Biogeochemical evidence for euxinic oceans and ecological disturbance presaging the end-Permian mass extinction event. Earth and Planetary Science Letters 281, 188–201.
Cao, C., Zheng, Q., 2009. Geological event sequences of the Permian-Triassic transition recorded in the microfacies in Meishan section. Science in China Series D: Earth Science 52, 1529–1536.
Chambers, L.A., Trudinger, P.A., 1979. microbial fractionation of stable sulfur isotopes: A review and critique. Geomicrobiology Journal. 1, 249–293.
Chen, J.-S., Chu, X.-L., 1988. Sulfur isotope composition of triassic marine sulfates of South China. Chemical Geology: Isotope Geoscience Section. 72, 155–161.
Claypool, G.E., Holser, W.T., Kaplan, I.R., Sakai, H., Zak, I., 1980. The age curves of sulfur and oxygen isotopes in marine sulfate and their mutual interpretation. Chemical Geology 28, 199–260.
Deshmukh, A.P., Chefetz, B., Hatcher, P.G., 2001. Characterization of organic matter in pristine and contaminated coastal marine sediments using solid-state 13C NMR, pyrolytic and thermochemolytic methods: a case study in the San Diego harbor area. Chemosphere 45, 1007–1102.
Detmers, J., Bruchert, V., Habicht, S.K., Kuever, J., 2001. Diversity of sulfur isotope fractionations by sulfate-reducing prokaryotes. Applied and Environmental Microbiology 67, 888–894.
Engel, M.H., Zumberge, J.E., 2007. Secular change in the stable sulfur isotope composition of crude oils relative to marine sulfates and sulfides. Book of Abstracts, International Meeting of Organic Geochemistry 2007 (Torquay, UK, September 19–24,). pp. 523–524.
Fossing, H., Jørgensen, B.B., 1989. Measurement of bacterial sulfate reduction in sediments: Evaluation of a single-step chromium reduction method. Biogeochemistry 8, 205–222.
Fry, B., Jannasch, H.W., Molyneaux, S.J., Wirsen, C.O., Muramato, J.A., King, S., 1991. Stable isotope studies of the carbon, nitrogen and sulfur cycles in the Black Sea and the Cariaco Trench. Deep-Sea Research Part a: Oceanographic Research Papers 38, S1003–S1019.

Goldhaber, M.B., Kaplan, I.R., 1980. Mechanisms of sulfur incorporation and isotope fractionation during early diagenesis in sediments of the gulf of California. Marine Chemistry 9, 95–143.
Greenwood, P.F., Amrani, A., Sessions, A., Raven, M.R., Holman, A.I., Dror, G., Grice, K., McCulloch, M.T., Adkins, 2014. J.F. In: Grice, K. (Ed.), RSC Detection Science Series No. 4: Principles and Practice of Analytical Techniques in Geosciences. Royal Society of Chemistry, Oxford, pp. 285–312.
Grice, K., Cao, C., Love, G.D., Bottcher, M.E., Twitchett, R.J., Grosjean, E., Summons, R. E., Turgeon, S.C., Dunning, W., Jin, Y., 2005. Photic zone euxinia during the Permian-triassic superanoxic event. Science 307, 706–709.
Grotheer, H., Greenwood, P.F., McCulloch, M.T., Böttcher, M.E., Grice, K., 2017. $\delta^{34}S$ character of organosulfur compounds in kerogen and bitumen fractions of sedimentary rocks. Organic Geochemistry 110, 60–64.
Habicht, K.S., Canfield, D.E., 1997. Sulfur isotope fractionation during bacterial sulfate reduction in organic-rich sediments. Geochimica et Cosmochimica Acta 61, 5351–5361.
Hallam, A., Wignall, P.B., 1997. Mass Extinctions and their Aftermath. Oxford University Press, p. 328.
Hartgers, W.A., Lopez, J.F., Sinninghe Damsté, J.S., Reiss, C., Maxwell, J.R., Grimalt, J. O., 1997. Sulfur-binding in recent environments: II. Speciation of sulfur and iron and implications for the occurrence of organo-sulfur compounds. Geochimica et Cosmochimica Acta 61, 4769–4788.
Hartmann, M., Nielsen, H., 2012. $\delta^{34}S$ values in recent sea sediments and their significance using several sediment profiles from the western Baltic Sea. Isotopes in Environmental and Health Studies. 48, 7–32.
Hay, W.W., Migdisov, A., Balukhovsky, A.N., Wold, C.N., Flögel, S., Söding, E., 2006. Evaporites and the salinity of the ocean during the Phanerozoic: Implications for climate, ocean circulation and life. Palaeogeography Palaeoclimatology Palaeoecology 240, 3–46.
Heinrichs, H., Brumsack, H.J., Loftfield, N., König, N., 1986. Verbessertes Druckaufschlußsystem für biologische und anorganische Materialien. Zeitschrift Für Pflanzenernährung und Bodenkunde. 149, 350–353.
Hongfu, Y., Kexin, Z., Jinnan, T., Zunyi, Y., Shunbao, W., Yin, H.F., Zhang, K.X., Tong, J. N., Yang, Z.Y., Wu, S.B., 2001. The Global Stratotype Section and Point (GSSP) of the Permian-Triassic Boundary. Episodes 24, 102–114.
Insalaco, E., Virgone, A., Courme, B., Gaillot, J., Kamali, M., Moallemi, A., Lotfpour, M., Monibi, S., 2006. Upper Dalan Member and Kangan Formation between the Zagros Mountains and offshore fars, Iran: depositional system, biostratigraphy and stratigraphic architecture. GeoArabia. 11, 75–176.
Jin, Y.G., Wang, Y., Wang, W., Shang, Q.H., Cao, C.Q., Erwin, D.H., 2000. Pattern of marine mass extinction near the Permian-Triassic boundary in South China. Science 289, 432–436.
Kaiho, K., Kajiwara, Y., Nakano, T., Miura, Y., Kawahata, H., Tazaki, K., Ueshima, M., Chen, Z., Shi, G.R., 2001. End-Permian catastrophe by a bolide impact: Evidence of a gigantic release of sulfur from the mantle. Geology 29, 815–818.
Kaiho, K., Chen, Z.Q., Kawahata, H., Kajiwara, Y., Sato, H., 2006a. Close-up of the end-Permian mass extinction horizon recorded in the Meishan section, South China: Sedimentary, elemental, and biotic characterization and a negative shift of sulfate sulfur isotope ratio. Palaeogeography Palaeoclimatology Palaeoecology. 239, 396–405.
Kaiho, K., Kajiwara, Y., Chen, Z.-Q., Gorjan, P., 2006b. A sulfur isotope effect at the end of the Permian. Chemical Geology 235, 33–47.
Kaiho, K., Oba, M., Fukuda, Y., Ito, K., Ariyoshi, S., Gorjan, P., Riu, Y., Takahashi, S., Chen, Z.Q., Tong, J.N., Yamakita, S., 2012. Changes in depth-transect redox conditions spanning the end-Permian mass extinction and their impact on the marine extinction: evidence from biomarkers and sulfur isotopes. Global and Planetary Change 94–95, 20–32.
Kaiho, K., Aftabuzzaman, M., Jones, D.S., Tian, L., 2020. Pulsed volcanic combustion events coincident with the end-Permian terrestrial disturbance and the followign global crisis. Geology 49, 289–293.
Kajiwara, Y., Yamakita, S., Ishida, K., Ishiga, H., Imai, A., 1994. Development of a largely anoxic stratified ocean and its temporary massive mixing at the Permian/Triassic boundary supported by the sulfur isotopic record. Palaeogeography Palaeoclimatology Palaeoecology 111, 367–379.
Kowalewski, I., Schaeffer, P., Adam, P., Dessort, D., Fafet, A., Carpentier, B., 2010. Formation of H_2S and sulfur-rich bitumen from a reservoired heavy oil in the presence of elemental sulfur. Organic Geochemistry 41, 951–998.
Kowalski, N., Dellwig, O., Beck, M., Grunwald, M., Dürselen, C.-D., Badewien, T.H., van Beusekom, J.E.E., Böttcher, M.E., 2012. A comparative study of manganese dynamics in pelagic and benthic parts of two tidal systems of the North Sea. Estuary, Coastal and Shelf Science 100, 3–17.
Li, C., Love, G.D., Lyons, T.W., Fike, D.A., Sessions, A.L., Chu, X., 2010. A Stratified Redox Model for the Ediacaran Ocean. Science 328, 80–83.
Newton, R.J., Pevitt, E.L., Wignall, P.B., Bottrell, S.H., 2004. Large shifts in the isotopic composition of seawater sulphate across the Permo-Triassic boundary in northern Italy. Earth and Planetary Science Letters 218, 331–345.
Nguyen, V.P., Burkl-Vitzthum, V., Marquaire, P.M., Michels, R., 2013. Thermal reactions between alkanes and H_2S or thiols at high pressure. Journal of Analytical and Applied Pyrolysis 103, 307–313.
Passier, H.F., Böttcher, M.E., De Lange, G.J., 1999. Sulphur enrichment in organic matter of eastern Mediterranean sapropels: A study of sulphur isotope partitioning. Aquatic Geochemistry 5, 99–118.
Price, F.T., Shieh, Y.N., 1979. Fractionation of sulfur isotopes during laboratory synthesis of pyrite at low temperatures. Chemical Geology 27, 245–253.
Raven, M.R., Adkins, J.F., Werne, J.P., Lyons, T.W., Sessions, A.L., 2015. Sulfur isotopic composition of individual organic compounds from Cariaco Basin sediments. Organic Geochemistry 80, 53–59.
Raven, M.R., Sessions, A.L., Fischer, W.W., Adkins, J.F., 2016. Sedimentary pyrite $\delta^{34}S$ differs from porewater sulfide in Santa Barbara Basin: Proposed role of organic sulfur. Geochimica et Cosmochimica Acta 186, 120–134.
Riccardi, A.L., Arthur, M.A., Kump, L.R., 2006. Sulfur isotopic evidence for chemocline upward excursions during the end-Permian mass extinction. Geochimica et Comsochimica Acta 70, 5740–5752.
Saito, R. Wörmer, L., Taubner, H., Kaiho, K., Takahashi, S. Tian, L., Ikeda, M., Summons, R. E., Hinrichs, K-U., 2023. Centennial scale sequences of environmental deterioration preceded the end-Permian mass extinction. Nature Communications 14, 2113.
Shawar, L., Halevy, I., Said-Ahmad, W., Feinstein, S., Boyko, V., Kamyshny, A., Amrani, A., 2018. Dynamics of pyrite formation and organic matter sulfurization in organic-rich carbonate sediments. Geochimica et Cosmochimica Acta 241, 219–239.
Shawar, L., Said-Ahmad, W., Ellis, G.S., Amrani, A., 2020. Sulfur Isotope composition of individual mcompounds in immature organic-rich rocks and possible geochemical implications. Geochimica et Cosmochimica Acta. 274, 20–44.
Song, H., Tong, J., Algeo, T.J., Song, H., Qiu, H., Zhu, Y., Tian, L., Bates, S., Lyons, T.W., Luo, G., Kump, L.R., 2014. Early Triassic seawater sulfate drawdown. Geochimica et Cosmochimica Acta 128, 95–113.
Werne, J.P., Lyons, T.W., Hollander, D.J., Formolo, M.J., Sinninghe Damsté, J.S., 2003. Reduced sulfur in euxinic sediments of the Cariaco Basin: Sulfur isotope constraints on organic sulfur formation. Chemical Geology 195, 159–179.
Werne, J.P., Lyons, T.W., Hollander, D.J., Schouten, S., Hopmans, E.C., Sinninghe Damsté, J.S., 2008. Investigating pathways of diagenetic organic matter sulfurization using compound-specific sulfur isotope analysis. Geochimica et Cosmochimica Acta 72, 3489–3502.
Whiteside, J.H., Grice, K., 2016. Biomarker Records Associated with Mass Extinction Events. Annual Reviews in Earth and Planetary Science. 44, 581–612.
Wignall, P.B., 2001. Large igneous provinces and mass extinctions. Earth-Science Reviews. 53, 1–33.
Wignall, P.B., Hallam, A., 1993. Griesbachian (Earliest Triassic) palaeoenvironmental changes in the Salt Range, Pakistan and southeast China and their bearing on the Permo-Triassic mass extinction. Palaeogeography Palaeoclimatology Palaeoecology 102, 215–237.
Wignall, P.B., Newton, R., 1998. Pyrite framboid diameter as a measure of oxygen deficiency in ancient mudrocks. American Journal of Science 298, 537–552.
Wilkin, R.T., Barnes, H.L., Brantley, S.L., 1996. The size distribution of framboidal pyrite in modern sediments: An indicator of redox conditions. Geochimica et Cosmochimica Acta 60, 3897–3912.
Worden, R.H., Smalley, P.C., Fallick, A.E., 1997. Sulfur cycle in buried evaporites. Geology. 25, 643–646.
Wortmann, U., Bernasconi, S., Bottcher, M., 2001. Hypersulfidic deep biosphere indicates extreme sulfur isotope fractionation during single-step microbial sulfate reduction. Geology. 29, 647–650.